PHYSICAL REVIEW B VOLUME 26, NUMBER 10 15 NOVEMBER 1982

X-ray form factors and the electronic structure of graphite

N. A. W. Holzwarth*
Corporate Research-Science Laboratories, Exxon Research and Engineering Company, Linden, New Jersey 07036

Steven G. Louie
Department of Physics, University of California, Berkeley, California 94720

Sohrab Rabii
University of Pennsylvania, Moore School of Electrical Engineering, Philadelphia, Pennsylvania 19104
(Received 23 February 1982)

The bonding and spectroscopic properties of graphite are investigated by carrying out first-principles, self-consistent electronic structure calculations, and by comparing the results with high-resolution data from recent x-ray diffraction and angle-resolved photoemission measurements. The theoretical valence-charge density is in excellent agreement with values derived from experimental x-ray form factors. Unlike other group-IV covalent materials, the bonding charge exhibits a prominent double-humped structure due to the lack of p core states. The energy band structure is also in good agreement with experimental measurements and previous calculations.

I. INTRODUCTION

Graphite intercalation compounds and adlayers of atoms on graphite have generated a great deal of theoretical and experimental interest in the past several years. These systems have potentially important technological applications, and they also provide realistic situations for the fundamental study of two-dimensional phenomena. As a consequence, renewed interest in the properties of graphite itself has been stimulated. There is, in fact, a very large literature on the electronic properties of graphite, including electron-density maps derived from x-ray diffraction data[1] and the energy-band measurements derived from high-resolution angle-resolved photoemission techniques.[2] There is also a very large number of theoretical calculations on the electronic structure of graphite. However, some features of the theoretical results are model dependent.

In the present paper we present the results of first-principles self-consistent calculations of the electronic structure of graphite, with the use of density-functional theory[3] in the local-density approximation[4] and mixed-basis pseudopotential techniques.[5] Our motivation is (1) to provide a deeper understanding of the bonding and spectroscopic properties of graphite and (2) to provide a basis of comparison for a study of graphite intercalation compounds using the same theoretical framework and computational techniques. Results for the intercalation compounds are published elsewhere.[6,7] The remainder of the paper is organized as follows. In Sec. II details of the calculation method are presented. In Sec. III the calculated distribution of valence-electron density is presented and compared with that derived from the analysis of x-ray diffraction experiments by Chen, Trucano, and Stewart.[1] The self-consistent valence density is also compared with that of superposed spherical atomic charge densities in order to illustrate aspects of the C—C bonding. In Sec. IV the calculated band structure is presented and compared with various spectroscopic measurements of band energies[2,8–10] and compared with a few of the previous calculations.[11–16] We do not attempt to make a thorough comparison of our band-structure results with the numerous results available in the literature, since this has been done by several other workers.[13–15] We are able, however, to understand how certain band features are sensitive to calculations methods, to self-consistency, and to the choice of the exchange-correlation approximation, as well as to establish our electronic structure of graphite as a credible one. Summary and conclusions are presented in Sec. V.

II. METHODS OF CALCULATION

The self-consistent band-structure calculations were carried out in the local-density approximation

and by representing the electron wave functions in terms of a mixed-basis set consisting of plane waves and linear combinations of atomic orbitals (LCAO's) as developed by Louie, Ho, and Cohen.[5] To take advantage of the numerical efficiency of a Fourier-space evaluation of the matrix elements, the calculations were formulated in terms of pseudopotentials and pseudo-wave-functions. The Hedin-Lundqvist[4] approximation for the exchange-correlation potential was used throughout this work.

A. Pseudopotential

We chose to use the norm-conserving pseudopotentials developed by Hamann, Schlüter, and Chiang.[17] This form of pseudopotential has the following advantages:

(1) the pseudopotential being energy independent over a reasonable energy range,

(2) the pseudo-wave-functions converging to the actual wave functions outside spheres of specified radii about each atom, and

(3) the integrated "pseudocharge" being equal to the integrated actual charge in the core regions.

Within the framework of the norm-conserving pseudopotentials of Hamann *et al.*,[17] there is some leeway in the choice of the functional form of the pseudopotentials in the core regions. For reasons of numerical efficiency, we have chosen a functional form that would ensure (a) that the Fourier transform of the pseudopotentials would have minimal extent as a function of reciprocal-lattice wave vector and (b) that the radial dependence of the nonlocal pseudopotential would have approximately Gaussian form. Since for the elements of interest in the present work, namely, C and Li, only *s*- and *p*-wave interactions are appreciable, we have followed the standard practice of approximating the *d*-wave and higher angular momenta interactions with the *s*-wave pseudopotential. This approximation has been proven to be reasonable for most semiconductors.

The *s*-wave atomic pseudopotentials were generated from the all-electron atomic potentials $V_A(r)$ using the following two-step procedure.[17] First the pseudopotential was set equal to the functional form

$$\Phi_0^{(1)}(r)=V_A(r)\{1-\exp[(-r/r_0')]\} +c_0\exp[-(r/r_0)^2] . \quad (1)$$

Here the constant c_0 was chosen so that the pseudopotential $\Phi_0^{(1)}(r)$ had a (nodeless) bound-state wave function $W_0^{(1)}(r)$ at the all-electron valence energy E_0. The pseudopotential radii r_0' and r_0 were chosen so that the pseudopotential would converge to the all-electron potential in the bonding region of the crystal. In the second step the pseudo-wave-function was modified so that it converged to the all-electron wave function for $r > r_l$, using the functional form

$$W_l^{(2)}(r)=\gamma_l W_l^{(1)}(r)+\delta_l r^l\exp[-(r/r_l)^2] , \quad (2)$$

where $l=0$ for s wave, and γ_l and δ_l are constants. The final atomic pseudopotential is then determined by inverting the Schrödinger equation for the pseudopotential corresponding to the pseudo-wave-function $W_l^{(2)}(r)$

$$\Phi_l^{(2)}(r)=\frac{\left[\frac{\hbar^2}{2m}\left[\frac{1}{r^2}\frac{d}{dr}r^2\frac{d}{dr}-\frac{l(l+1)}{r^2}\right]+E_l\right]W_l^{(2)}(r)}{W_l^{(2)}(r)} \quad (3)$$

The *p*-wave pseudopotential was generated by a similar two-step procedure, except that, for numerical reasons, in order to simplify the nonlocal potential contributions, the first-step *p* pseudopotential was taken to be of the form

$$\Phi_1^{(1)}(r)=\Phi_0^{(2)}(r)+c_1\exp[-(r/r_1)^2] . \quad (4)$$

Once the neutral atomic pseudopotentials were obtained, the ionic pseudopotentials $\Phi_0^I(r)$ and $\Phi_1^I(r)$ were determined[17] by subtracting the valence-electron screening potentials due to Hartree and exchange-correlation interactions. The configuration $2s^1p^3$ was used to generate the carbon pseu-

TABLE I. Numerical parameters used in computation.

Pseudopotential parameters		Carbon	Lithium
r_0 $(=r_0')$	[Eq. (1)]	0.7 bohr	1.5 bohr
r_l	[Eq. (4)]	0.55 bohr	1.5 bohr
q_1^2	[Eq. (11)]	2.1 bohr^{-2}	0.35 bohr^{-2}
Basis-set parameters			
Plane waves		$0\le \lvert\vec{k}+\vec{G}\rvert^2\le 3$ bohr^{-2}	
Fourier expansion of localized orbitals		$0\le \lvert\vec{k}+\vec{G}\rvert^2\le 25$ bohr^{-2}	

dopotential, and the configuration $2s^{1/2}2p^{1/2}$ was used to generate the lithium pseudopotential; however, several other atomic configurations yielded virtually the same ionic pseudopotentials. The pseudopotential parameters used in the present work are listed in Table I.

B. Numerical methods of the mixed-basis band-structure calculations

The numerical methods used in the present work are for the most part described in Ref. 5. The orbitals used to construct the LCAO components of the basis set were the valence-electron pseudo-wavefunctions with radial components $W_l^{(2)}(r)$ described above. For both C and Li, LCAO Bloch functions were constructed for each of the s and p valence orbitals. The convergence requirements of the basis set in the present work were determined primarily by the C pseudopotentials. Therefore, it was appropriate to check convergence using the diamond band structure. Using the range of plane waves and the range of reciprocal-space expansion of the LCAO wave functions listed in Table I, eigenvalues were converged to within a maximum error of 0.2 eV.[18] It was necessary to permit this relatively large error in order to keep the computation time within reason for the high-stage intercalation compounds. We found our choice of numerical LCAO functions to be preferable to Gaussian orbitals. In a limited test using the diamond band structure, we found that the use of single Gaussian LCAO's required the inclusion of more plane waves to achieve comparable convergence.

Because the local orbitals $W_l^{(2)}(r)$ extend beyond a single site, the on-site approximation described in Ref. 5 could not be used in the present work. Consequently, the most time consuming part of the calculation was the evaluation of matrix elements of the pseudopotential between LCAO functions. The matrix elements of the local pseudopotentials (s-wave part of ionic pseudopotentials plus Hartree and exchange-correlation contributions of the valence electrons) were evaluated using the fast-Fourier-transform technique. This technique is essentially an efficient trapezoidal-rule integration throughout the unit cell. The integration mesh is determined by the inverse of the maximum reciprocal-space range $Q_{\max}$ of the matrix-element components. The component having the largest reciprocal-space range in the present work is the C s-wave ionic pseudopotential with $Q_{\max}\approx 8$ bohr^{-1}.

The contributions of the nonlocal pseudopotential (p-wave ionic pseudopotential minus s-wave ionic pseudopotential) to the matrix elements were evaluated using a separable-form approximation described below. The matrix element of the nonlocal pseudopotential between two LCAO basis functions, with Fourier components denoted by $W_i(\vec{q})$, is given by

$$\langle i \mid V_{\rm NL} \mid j \rangle = \sum_{\vec{G},\vec{G}'} W_i^*(\vec{k}+\vec{G}) V_{\rm NL}(\vec{k}+\vec{G},\vec{k}+\vec{G}') \times W_j(\vec{k}+\vec{G}') , \quad (5)$$

where $V_{\rm NL}(\vec{k}+\vec{G},\vec{k}+\vec{G}')$ is the plane-wave matrix element of the nonlocal potential. The idea of the separable form is that the plane-wave matrix element is approximated by

$$V_{\rm NL}(\vec{k}+\vec{G},\vec{k}+\vec{G}') \approx \sum_{\mu,\nu=0}^{M} A_{\mu\nu} f_\mu^*(\vec{k}+\vec{G}) f_\nu(\vec{k}+\vec{G}') , \quad (6)$$

where $f_\nu(\vec{k}+\vec{G})$ are specified functions and $A_{\mu\nu}$ are constant coefficients, so that Eq. (5) becomes

$$\langle i \mid V_{\rm NL} \mid j \rangle \approx \sum_{\mu,\nu=0}^{M} A_{\mu\nu} F_\mu^{i*} F_\nu^j , \quad (7)$$

with

$$F_\nu^j \equiv \sum_{\vec{G}'} f_\nu(\vec{k}+\vec{G}') W_j(\vec{k}+\vec{G}') . \quad (8)$$

Provided that the number of significant coefficients $A_{\mu\nu}$ are kept small, Eq. (7) is then more efficient to evaluate than the direct form [Eq. (5)].

The plane-wave matrix element of the nonlocal potential is given by

$$V_{\rm NL}(\vec{k}+\vec{G},\vec{k}+\vec{G}') = \frac{(4\pi)^2}{\Omega} \sum_{\tau l} e^{-i(\vec{G}-\vec{G}')\cdot\vec{\tau}} \Phi_l^\tau(\mid \vec{k}+\vec{G} \mid, \mid \vec{k}+\vec{G}' \mid) \sum_M Y_{lM}^*(\hat{k}_G) Y_{lM}(\hat{k}_{G'}) , \quad (9)$$

where

$$\Phi_l^\tau(\mid \vec{k}+\vec{G} \mid, \mid \vec{k}+\vec{G}' \mid) \equiv \int_0^\infty r^2 dr\, j_l(\mid \vec{k}+\vec{G} \mid r) j_l(\mid \vec{k}+\vec{G}' \mid r) [\Phi_{\tau l}^I(r) - \Phi_{\tau 0}^I(r)] . \quad (10)$$

In Eqs. (9) and (10) Ω is the unit-cell volume, τ represents the atomic site, l represents the angular momentum of the nonlocal potential ($l=1$ in the present work), and $\hat{k}_G \equiv (\vec{k}+\vec{G})/|\vec{k}+\vec{G}|$. It is apparent from Eq. (9) that the separable approximation need only be made to the function $\Phi_l^\tau(q,q')$, since the other factors are already in separable form. The choice of separable functions is not unique. Our choice was

$$\Phi_l^\tau(q,q') \simeq \sum_{n,n'=0}^{N} \mathscr{C}_{nn'}^{\tau l}\{\exp[-(q^2+q'^2)/4q_{\tau l}^2]\} q^{l+2n}(q')^{l+2n'} , \tag{11}$$

where

$$\mathscr{C}_{nn'}^{\tau l} \equiv \sum_{\nu=0}^{n}\sum_{\nu'=0}^{n'} \mathscr{E}_{n-\nu} J_\nu \mathscr{E}_{n'-\nu'} J_{\nu'} \int_0^\infty r^2 dr\, r^{2l+2\nu+2\nu'}[\Phi_{\tau l}^I(r) - \Phi_{\tau 0}^I(r)] ,$$

$$\mathscr{E}_n \equiv [n!(4q_{\tau l}^2)^n]^{-1} \text{ and } J_n = [(-2)^n n!(2l+2n+1)!!]^{-1} .$$

This form of the separable function has one adjustable parameter for each nonlocal potential, the range parameter $q_{\tau l}$. The expansion (11) is absolutely convergence when the radial part of the nonlocal potential takes the Gaussian form $\exp(-q_{\tau l}^2 r^2)$. We found this choice of separable functions using $q_{\tau l} \approx r_{\tau l}^{-1}$ to be adequate for both C and Li, although care had to be exercised for possible divergences at large q. Here $r_{l\tau}$ is the pseudopotential radius defined in Eqs. (1) and (2).

The charge density of the occupied states for each iteration in the self-consistent process was evaluated as described in Ref. 5. Because of the existence of partly filled bands, midpoint sampling algorithms were more appropriate than special point algorithms, since the latter are heavily dependent upon the continuity of the integrand and of its derivatives. For LiC_{12} and LiC_{18}, a 19-point midpoint sampling was used within the irreducible sectors ($\frac{1}{4}$) of the Brillouin zones. Equivalent or better samplings were used for LiC_6 and graphite.

III. VALENCE-ELECTRON-DENSITY DISTRIBUTION

Graphite has the Bernal[19] structure with D_{6h}^4 symmetry and four atoms and two inequivalent types per unit cell. The atoms are arranged in layers of hexagonal lattices with lattice constant $a=2.46$ Å; the separation between layers is $c/2=3.35$ Å. Adjacent layers are shifted in an *ABAB* stacking such that half of the carbon atoms (type *a*) are directly above and below carbon atoms in the adjacent layers, while half (type *b*) are directly above and below centers of carbon hexagons in the adjacent layers.

Graphite is one of the few materials for which a detailed analysis of the x-ray diffraction data has been performed in terms of the valence-electron density.[1] In Fig. 1(a), the results of our self-consistent electronic structure calculations for the valence-electron density is presented in comparison with the density generated by the most refined fit to the x-ray form factors[1] [Fig. 1(b)]. The overall agreement between the two density distributions is excellent: $\pm 0.15 e/\text{Å}^3$ throughout the entire unit cell, close to the experimental accuracy. The experimental density is generally higher than the calculated density. A contributing factor to this trend is the fact that the experimental fitting parameters were not constrained to the total number of electrons. The set of parameters[1] used to generate

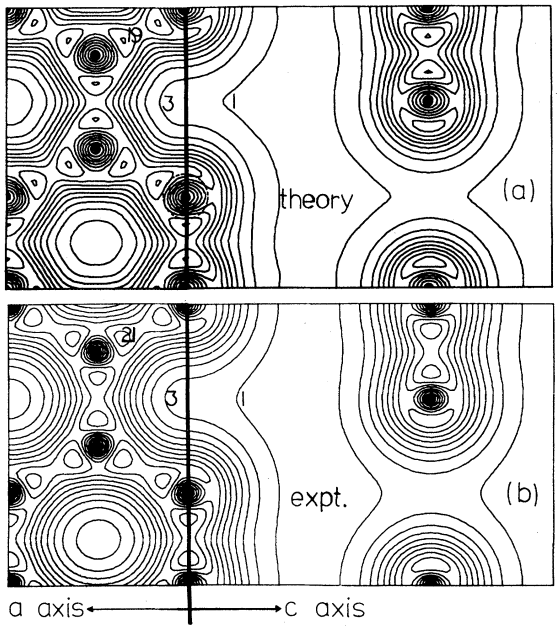

FIG. 1. Contour plots of valence-electronic-charge density for graphite: (a) Present results, and (b) results from analysis of x-ray data by Chen, Trucano, and Stewart (Ref. 1). Contour values are given in units of $0.1e/\text{Å}^3$. Atomic positions are denoted by filled circles. Two planes are shown—one containing an *a* axis and the other containing the *c* axis and both intersecting at 90° along a C—C bond. In (a) the dashed circle denotes the pesudopotential radius. In (b) the authors quote a standard deviation of $\pm 0.1e/\text{Å}^3$.

Fig. 1(b) overestimates the total density by $0.034e/\text{Å}^3$. Since ours is a pseudocharge density, the shape of the density within the pseudopotential radius [indicated in Fig. 1(a) by a dashed circle] is not simply related to the real electron density. However, the integral of the real charged within the same region.[17] The experimental determination of the valence charge near the core region is also somewhat less accurate since the core contribution has been assumed to have a particular form and did not enter into the experimental fit. The difference between the two distinct carbon sites is very slight—negligible in the calculated density and smaller than the standard deviation in the experimentally derived density. This indicates that the ground-state density is rather insensitive to the interlayer structure. This insensitivity was also shown by Posternak, Wimmer, and Freeman[20] who reported favorable agreement of their calculated electron density for a single graphite layer with the experimental results of Ref. 1.

Figure 1 illustrates the highly anisotropic structure of the graphite valence density and the large concentration of charge that constitutes the C—C bonds. The density along the bond exhibits a double-humped feature with peak densities of roughly $2.1e/\text{Å}^3$, 10% higher than the density at the bond center. This distinctive feature of the C—C bond has also been seen in diamond[21,22] and is very likely to be due to the competing effects of the s- and p-wave ionic pseudopotentials. For carbon, the p-wave ionic pseudopotential is significantly more attractive than is the s-wave ionic pseudopotential. For group IV, materials in the third and higher rows of the Periodic Table, such as Si, Ge, and Sn, the existence of p-core states causes the p and s pseudopotentials to have roughly equal strength and the covalent bonds do not exhibit a double-humped feature.

It is informative to consider the formation of the graphite bonds by comparing the experimental density with that due to the superposed density of spherical carbon atoms as shown in Fig. 2. Even though the atomic configuration has been taken as sp^3 (sp^2 plus p_z), the superposed density is not nearly as concentrated along the bonding directions as is the actual graphite density. The superposed density has a peak of $1.8e/\text{Å}^3$ in a nearly spherical region about each carbon atom in contrast to the higher peak values along bond directions exhibited in the actual graphite density. The maximum density at the midpoint of the C—C bond is 30% smaller for the superposed density than that of graphite.

From the Coulombic and exchange-correlation potentials generated from the superposed atomic valence density of Fig. 2 and the ionic pseudopotentials of the C^{4+} ions, one obtained the first-iteration charge density shown in Fig. 3. From this figure, it is apparent that the first-iteration charge density is close to that of the final-iteration density shown in Fig. 1(a) and within the standard deviation of the experimental density shown in Fig. 1(b). Within this point of view, it is apparent that the ionic potentials are the dominant factor which concentrate charge in the bond region of graphite and that the precise shape of the screening charge plays a secondary role. On a somewhat finer scale, we can compare the first- (Fig. 3) and last- [Fig. 1(a)] iteration charge densities to see that the first-iteration density is overconcentrated in the bond region. The self-consistent density is slightly more extended into the nonbonding regions. This behavior is also reflected in changes in the energy bands as a function of iteration, as will be discussed in Sec. IV.

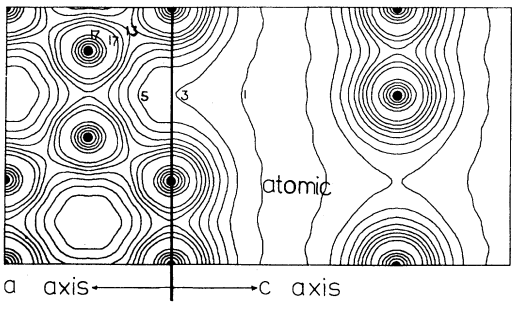

FIG. 2. Contour plot of superposed valence-electron-charge density of sp^3 carbon atoms in the graphite structure. Contour values are given in units of $0.1e/\text{Å}^3$. Atomic positions are denoted by filled circles. The two planes shown are as in Fig. 1.

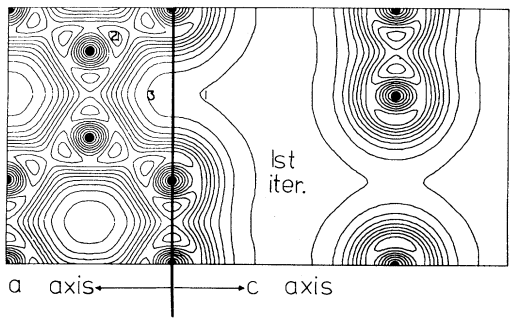

FIG. 3. Contour plot of first-iteration valence-electronic-charged graphite in units of $0.1e/\text{Å}^3$. Atomic positions are denoted by filled circles. The two planes shown are as in Figs. 1 and 2.

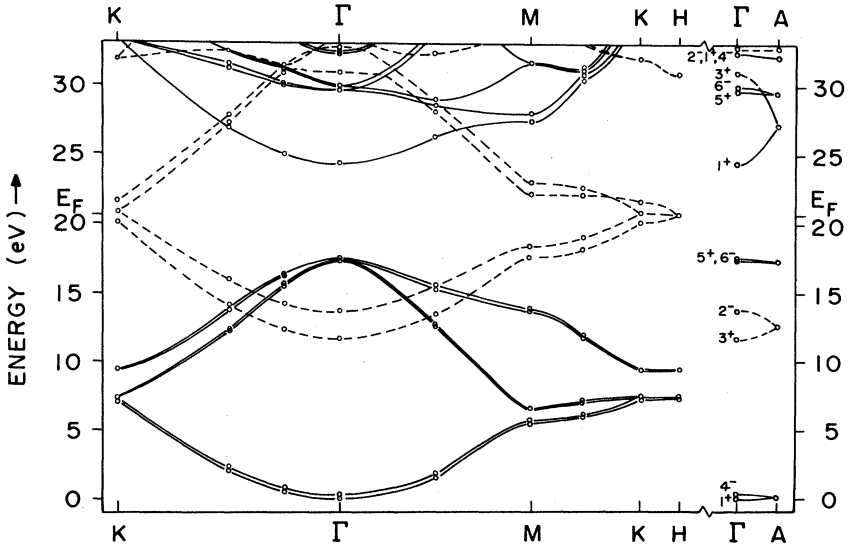

FIG. 4. Self-consistent band structure of graphite (Hedin-Lundqvist exchange-correlation potential). Dashed lines denote π bands, solid lines denote σ bands.

IV. BAND STRUCTURE

The band structure of graphite has been reported by many authors. Within these reported results, there are 1—2-eV variations in the calculated σ- and π-band extrema, and in the splitting of the π bands due to interlayer interactions. It is our opinion that most of the calculated band dispersions are generally consistent with the available experimental data. However, as will be discussed below, we can identify some of the factors which cause these discrepancies.

TABLE II. Band energies (in eV) for graphite.

	Present results		Previous calculations		Experimental
	Hedin-Lundqvist	Slater			
Γ-point states					
bottom σ band[a]	0	0	0[b]	0[c]	0[d]
	0.3	0.2	0.5[b]	0.3[c]	
bottom π band	11.7	12.9	12.5[b]	11.3[c]	12.5[d]
	13.7	14.5	14.2[b]	13.0[c]	13.4[d], 16.8[e]
top σ band	17.4	17.2	16.1[b]	15.2[c]	16.0[d]
	17.5	17.4		15.2[c]	
unoccupied σ bands	24.5	26.9	28.3[b]	26.6[c]	
	29.8	30.1	28.0[b]	26.8[c]	27.5[f]
	30.1	30.4	28.7[b]	26.8[c]	
E_F	20.8	21.5	20.5[b]	19.5[c]	20.6[d], 22.5[e]
π bands near E_F[g]					
$E_2^0-E_3^0$	0.7	0.5	0.44[h]	0.44[c]	0.72[i]
$E_3^0-E_1^0$	0.8	0.6	0.55[h]	0.61[c]	0.84[i]

[a]Lowest σ band chosen as zero of energy; all energies in eV.
[b]Reference 12.
[c]Reference 13.
[d]Angle-resolved photoemission, Ref. 2.
[e]Angle-integrated photoemission, Ref. 10.
[f]Reference 8.
[g]Notation of Slonczewski and Weiss, Ref. 23.
[h]Reference 11.
[i]Reference 9.

The present band-structure results calculated using the Hedin-Lundqvist[4] exchange and correlation potentials are given in Fig. 4. Various features of our results[18] are compared with some previous calculations and experiments in Table II. In general, the present results for the occupied bands are consistent with the previous literature. The splitting of the bands at the K point near the Fermi level is in good agreement with experiment although the detailed 0.01-eV dispersions of the Fermi-level bands along the K-H direction[14,23] are beyond the accuracy of the present calculations. The total valence-band width (20.8 eV), the σ-band width (17.3 eV), and the σ-π band separations [12.7 eV (bottom) and 4.8 eV (top)] are within a few electron volts of previous calculations[11–16] and of angle-resolved photoemission measurements.[2] In fact, the spread in previously calculated results, as well as the uncertainties introduced in the photoemission process in determining these high-binding energy-band features, are also on the order of a few electron volts. We find that the bottom of the π band is split by 2.0 eV due to interlayer interactions, whereas the σ bands (which are highly concentrated near the carbon layers) are being split considerably less. The present value of the π-band splitting is consistent with previous calculations[11–16] but twice that inferred from photoemission.[2] The photoemission value is a lower limit due to the effects of c-axis dispersion which enter for the geometry of the experiment.

The most puzzling feature of the present results is the location of the first unoccupied σ band. This band, which has a band minimum of character Γ_1^+, is of particular importance to the Li intercalation compounds since it would strongly hybridize with the bottom of the Li 2s band. In our results, using the Hedin-Lundqvist exchange-correlation approximation, this Γ_1^+ band is 2–4 eV below previously calculated values. However, since this feature is the minimum of a parabolic band, it may not be experimentally detectable. The band contributes a very low density of states and is, therefore, not easily detected in reflectivity measurements.[24,25] Moreover, it would be located below the vacuum level so as not to be accessible to photoemission measurements. An examination of the electron-density distribution for this state shows that it has an extra node near each carbon ion and is highly concentrated in the region between the two carbon planes. In LCAO language, one would be tempted to label this state as the bottom of the carbon 3s band. We find that the inclusion of plane waves in the mixed-basis set is essential to the proper description of this state; their omission significantly shifts its energy position. The Γ_1^+ state for an inadequate basis set is forced to have a higher energy than it does in a converged basis expansion such as used in the present work. However, basis-set completeness does not explain the entire discrepancy; a recent Korringa-Kohn-Rostoker calculation, in which muffin-tin corrections were included and all expansions were well converged,[13] showed this state to be 2 eV higher than in the present results. As will be discussed below, the remaining discrepancy can be attributed partly to self-consistency and partly to the use of different exchange-correlation approximations.

The effects of self-consistency on the band energies (at the zone center) are illustrated in Fig. 5. The diagram on the left of the figure illustrates the results for graphite using the Hedin-Lundqvist exchange-correlation approximation.[4] The three diagrams on the right of the figure present the analogous results for three stages of Li-intercalated graphite. The extra bands in the Li-intercalated compounds are caused by zone folding due to the Li superlattice. It is interesting to note that the trends seen in the intercalation compounds are similar to that seen in graphite itself. This can be understood since Li only contributes one electron compared with 24, 48, or 72 carbon electrons, respectively, for stage-1, -2, and -3 Li-intercalated graphite. Thus

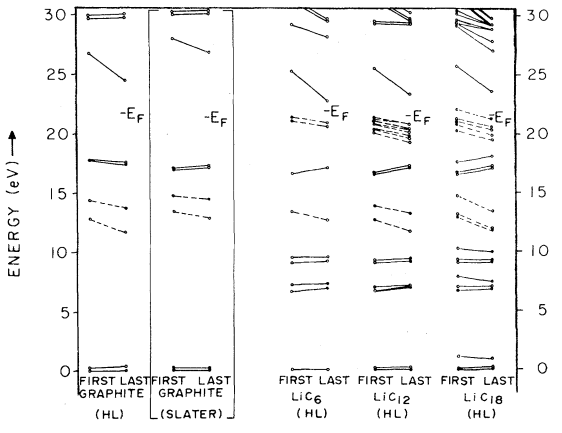

FIG. 5. Energy-level diagram showing the effects of self-consistency on the Γ-point levels for the first-iteration (FIRST) and self-consistent (LAST) potentials. HL denotes Hedin-Lundqvist exchange-correlation approximation, while SLATER denotes Slater's approximation. The last three panels of the figure show the results for three stages of Li-intercalated graphite. Dashed lines denote π bands, solid lines denote σ bands.

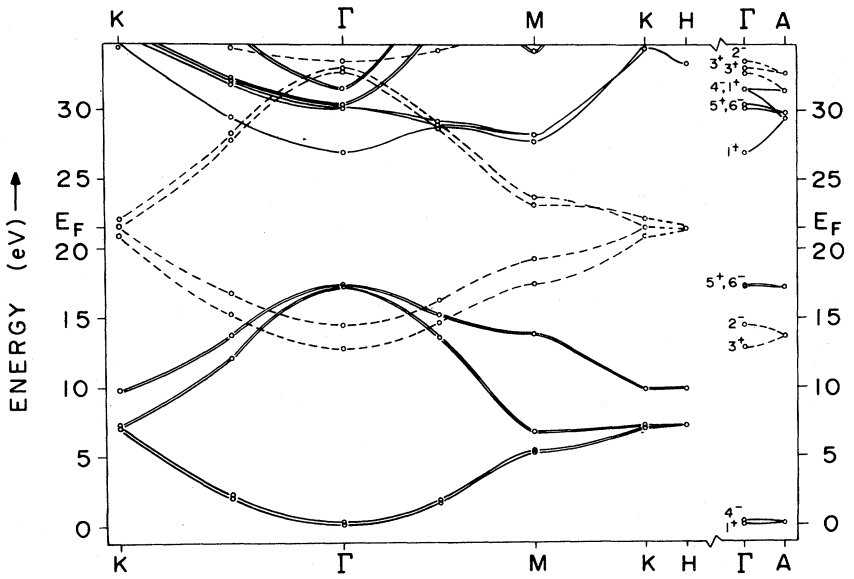

FIG. 6. Self-consistent band structure of graphite for Slater's exchange-correlation approximation. Dashed lines denote π bands, solid lines denote σ bands.

the major changes in the self-consistency process are those for the carbon electrons.

The energy shifts between the non-self-consistent and self-consistent energy-bands result from the charge-density changes shown in Figs. 1—3. Namely, the superposed atomic density (Fig. 2) is too diffuse to self-consistently screen the ionic potential of the crystal. The resulting first-iteration charge density (Fig. 3) is overconcentrated in the bonding regions. (The corresponding energy bands are shown in the far-left portion of Fig. 5.) By the final iteration, the charge [Fig. 1(a)] has relaxed slightly into the nonbonding regions, and the π bands become lowered in energy. The unoccupied Γ_1^+ band is lowered by 3 eV in energy during the self-consistency iteration. The lowering of the energy of the π and Γ_1^+ states, which have appreciable extent in the region between the carbon planes, is affected mainly by the exchange-correlation potential which becomes more attractive with increasing electron density. It is important to have a complete basis set to correctly describe the self-consistent screening charge.

The effects of the exchange-correlation approximations on the bands of graphite were studied by performing a self-consistent calculation using Slater's exchange approximation.[26] The Hedin-Lundqvist exchange-correlation potential is generally less attractive than the Slater exchange potential by a density-dependent factor that varies from $\frac{2}{3}$ (at high density) to 1.2 (at low density). For the densities appropriate to graphite, the factor varies only from 0.7 in the bonding region to 0.9 between carbon planes. As a result, the Slater exchange-correlation potential is systematically more attractive in the bonding region so that the self-consistent density is more concentrated in the bonding regions than is the density derived from the Hedin-Lundqvist form. The resulting zone-center eigenvalues are illustrated in the second panel of Fig. 5 and the complete band structure is given in Fig. 6. The band energies are also listed in the second column of Table II. It is evident that concentration of the wave functions of the occupied states into the bonding region causes the splitting of the bottom of the π band to decrease by 0.5 eV and causes the unoccupied Γ_1^+ band to move up by 2.5 eV in energy. The splitting of the bands near the Fermi level for the Slater approximation is in slightly poorer agreement with experiment than is the splitting for the Hedin-Lundqvist approximation.

V. SUMMARY

This study has demonstrated that self-consistent local-density calculations for graphite are capable of determining electron-charge-density distributions in

quantitative agreement with experiment. Although the Hedin-Lundqvist form of the exchange-correlation function is a more sophisticated approximation than is the Slater function, both results are consistent with the x-ray data, as is the first-iteration (non-self-consistent) charge density. The energy bands are somewhat more sensitive to these factors, and the self-consistent Hedin-Lundqvist bands agree best with experimental determination of the bands near the Fermi level. We have successfully established our results as a reasonable basis of comparison for intercalation compounds of graphite.

ACKNOWLEDGMENTS

We would like to thank R. C. Tatar and J. R. Chelikowsky for helpful discussions, and A. J. Freeman and M. A. Posternak for pointing out Ref. 1. This work was supported by National Science Foundation Materials Research Laboratory Grant No. DMR79-23647, Army Research Office Contract DAAG-29-77-C400, and National Science Foundation Grant No. DMR78-22465. One of us (S.G.L.) would like to acknowledge support from a Sloan Foundation Fellowship.

*Present address: Department of Physics, City College of CUNY, Convent Avenue at 138 St., New York, N.Y. 10031.

[1]R. Chen, P. Trucano, and R. F. Stewart, Acta Crystallogr. Sect. A 33, 823 (1977).

[2]W. Eberhardt, I. T. McGovern, E. W. Plummer, and J. E. Fischer, Phys. Rev. Lett. 44, 200 (1980).

[3]P. Hohenberg and W. Kohn, Phys. Rev. 136, B864 (1964); W. Kohn and L. J. Sham, *ibid.* 140, A1133 (1965).

[4]L. Hedin and B. I. Lundqvist, J. Phys. C 4, 2064 (1971).

[5]S. G. Louie, K. M. Ho, and M. L. Cohen, Phys. Rev. B 19, 1774 (1979).

[6]N. A. W. Holzwarth, S. G. Louie, and S. Rabii, Phys. Rev. Lett. 47, 1318 (1981).

[7]N. A. W. Holzwarth, S. G. Louie, and S. Rabii (unpublished).

[8]R. F. Willis, B. Feuerbacher, and B. Fitton, Phys. Rev. B 4, 2441 (1971).

[9]G. Bellodi, A. Borghesi, G. Guizzetti, L. Nosenzo, E. Reguzzoni, and G. Samoggia, Phys. Rev. B 12, 5951 (1975).

[10]A. Bianconi, S. B. M. Hagström, and R. Z. Bachrach, Phys. Rev. B 16, 5543 (1977).

[11]G. S. Painter and D. F. Ellis, Phys. Rev. B 1, 4747 (1970).

[12]R. F. Willis, B. Fitton, and G. S. Painter, Phys. Rev. B 9, 1926 (1974).

[13]R. C. Tatar and S. Rabii, Phys. Rev. B 25, 4126 (1982).

[14]A. Zunger, Phys. Rev. B 17, 626 (1978).

[15]I. L. Spain, in *Chemistry and Physics of Carbon,* edited by P. L. Walker and P. A. Thrower (Dekker, New York, 1973), Vol. 8, p. 1.

[16]H. Nagayoshi, K. Nakao, and Y. Uemura, J. Phys. Soc. Jpn. 41, 1480 (1976).

[17]D. R. Hamann, M. Schlüter, and C. Chiang, Phys. Rev. Lett. 43, 1494 (1979).

[18]The self-consistency of our calculated energy levels and the relative positions among levels were converged to well within 0.05 eV. The absolute position of the levels, on the other hand, were converged to within 0.2 eV. This relatively large error was permitted in order to keep the calculations for the stage-3 intercalation compound within a reasonable computation time.

[19]J. D. Bernal, Proc. R. Soc. London, Ser. A 106, 749 (1924).

[20]M. A. Posternak, E. Wimmer, and A. J. Freeman, Bull. Am. Phys. Soc. 26, 483 (1981).

[21]M. T. Yin and M. L. Cohen, Phys. Rev. B 24, 6121 (1981).

[22]A. Zunger and A. J. Freeman, Phys. Rev. B 15, 5049 (1977).

[23]J. C. Slonczewski and P. R. Weiss, Phys. Rev. 109, 272 (1958); J. W. McClure, *ibid.* 108, 612 (1957).

[24]E. A. Taft and H. R. Philipp, Phys. Rev. 138, A197 (1965).

[25]D. L. Greenway, G. Harbeke, F. Bassani, and E. Tosatti, Phys. Rev. 178, 1340 (1969).

[26]J. C. Slater, Phys. Rev. 81, 385 (1951); 82, 538 (1951).